Prediction of pattern selection due to an interaction between longitudinal rolls and transverse modes in a flow through a rectangular channel heated from below

Yuki Kato* and Kaoru Fujimura
Department of Applied Mathematics and Physics, Tottori University, Tottori 680-8552, Japan
(Received 18 October 1999)

Convection patterns in a flow through a horizontal channel that is heated from below are predicted on the basis of a weakly nonlinear theory. At a certain value of the Reynolds number and the Rayleigh number, the conduction state with steady shear flow becomes linearly unstable to both longitudinal rolls and transverse modes, simultaneously. The longitudinal rolls align along the streamwise direction whereas the transverse modes are periodic in the streamwise direction. Amplitude equations for the interaction between the longitudinal rolls and the transverse modes are derived in a consistent manner. Coefficients in the equations are determined numerically for a wide range of parameters. The longitudinal rolls are found to bifurcate supercritically. On the other hand, the transverse modes bifurcate subcritically or supercritically, depending on the Prandtl number, the aspect ratio of the channel, and the boundary conditions on the sidewalls. Stable convection patterns are classified in a parameter space. A mixed mode pattern, which is a mixture of the components of the longitudinal rolls and the transverse modes, is found to be stable for some sets of parameters.

PACS number(s): 47.20.Bp, 47.54.+r, 47.20.Ky, 47.60.+i

I. INTRODUCTION

Rayleigh-Bénard convection with superimposed through flow is of interest in many fields of science and engineering. In particular, a practical interest is growing in thermal CVD (chemical vapor deposition) of compound films. The uniformity of film thickness is influenced by the convection patterns in the CVD reactors [1]. Spatiotemporal patterns of convection depend on parameters characterizing the thermal stratification and the through flow: the Rayleigh number Ra, the Prandtl number Pr, the Reynolds number Re, and the aspect ratio of the channel. Our goal is to determine the convection patterns achieved for a given set of these parameters.

We begin by considering an unstably stratified layer of Boussinesq fluid between two horizontal parallel plates of infinite extent. If no through flow exists, the conduction state is isotropic and homogeneous in the horizontal plane. Convection rolls, caused by thermal instability, may therefore align in arbitrary directions. When a steady shear flow is superimposed, the preferred rolls align along the streamwise direction. The imposed shear thus exerts pattern selection mechanism on the convection rolls. When the Reynolds number of the through flow exceeds the critical value Re_c, the hydrodynamic instability causes Tollmien-Schlichting waves. The critical Reynolds number increases as the Rayleigh number decreases, and $\mathrm{Re}_c = 5772.2218$ at $\mathrm{Ra} = 0$. See Gage and Reid [2] or Kelly [3], for instance.

In what follows, we call the instability mode longitudinal if it aligns along the streamwise direction. We call the mode transverse if it is periodic and its wave-number vector is parallel to the superimposed flow. Previous analyses of the linear stability concluded that, under the influence of the shear flow, the most unstable thermal convection rolls are longitudinal. The most unstable Tollmien-Schlichting waves are transverse. On a linear basis, both the longitudinal rolls and the transverse modes can set in simultaneously, at certain values of the Reynolds number ($\mathrm{Re} = \mathrm{Re}_*$, say) and the Rayleigh number ($\mathrm{Ra} = \mathrm{Ra}_*$). We shall call ($\mathrm{Re}_*, \mathrm{Ra}_*$) a crossover point in the Re-Ra plane. In the neighborhood of the crossover point, the linear stability theory loses its validity to predict convection patterns. This is because a nonlinear interaction between the two coexisting modes plays a significant role in pattern selection. The interaction may produce a new pattern, a mixture of the components of the longitudinal rolls and the transverse modes. We call this the mixed mode pattern. The question then arises: which pattern is stable—the longitudinal rolls, the Tollmien-Schlichting waves, or the mixed mode pattern? Weakly nonlinear analysis revealed that stable convection patterns involve the longitudinal rolls and the mixed mode pattern [4].

As well as the shear flow, the finiteness of the horizontal extent also exerts a pattern selection mechanism. Davis [5] examined the linear stability of the conduction state in a three-dimensional enclosure. He assumed a quasi-two-dimensional disturbance with two nonzero velocity components depending on all spatial variables. The preferred pattern was concluded to consist of the rolls aligned along the shorter sidewalls. The quasi-two-dimensional disturbance does not exactly satisfy the linearized disturbance equations, as was proved by Davies-Jones [6]. Nevertheless, the quasi-two-dimensional disturbance gives a close approximation of the preferred patterns in some cases.

Let us now consider a flow in a rectangular channel with infinite length. The Davis result suggests that, in the absence of through flow ($\mathrm{Re} = 0$), the preferred pattern consists of thermal convection rolls, which align along the spanwise direction. This was confirmed in Ref. [6] for a channel with free horizontal walls and rigid sidewalls. When we superimpose a through flow, the convection rolls aligned along the spanwise direction lie across the flow. The critical Rayleigh number for these transverse modes increases as Re increases [7,8]. That is, the through flow stabilizes the conduction state against the transverse modes. The through flow has, on the

*Email address: kato@damp.tottori-u.ac.jp

contrary, no effect on the critical condition for the longitudinal rolls. The critical Rayleigh number for the longitudinal rolls is exactly the same as the critical Rayleigh number for the convection in a two-dimensional box [9–11]. As a result, the critical mode is transverse for sufficiently small Re, and longitudinal for large Re. As above, the effects of the sidewalls and the through flow compete. A crossover thus occurs between the longitudinal rolls and the transverse modes, both of which are due to the thermal instability. When the aspect ratio of the channel exceeds 3.2, nonuniform shear may drive the hydrodynamic instability: Tollmien-Schlichting waves set in for much larger Re [12]. The crossover between the Tollmien-Schlichting waves and longitudinal rolls is, however, beyond the scope of the present paper.

In the neighborhood of the crossover point $(\mathrm{Re}_*, \mathrm{Ra}_*)$, nonlinear interaction between the coexisting thermal convection modes may form a mixed mode pattern. To predict the stable patterns achieved in a channel with finite aspect ratio, heavy numerical work is unavoidable even on a weakly nonlinear basis. To avoid the difficulty, Brand *et al*. introduced model equations [13], whereas Müller *et al*. modeled the effect of the sidewalls [14]. Both of their analyses are based on envelope equations. Brand *et al*. show that mixed modes may be stable in addition to the longitudinal rolls and transverse modes. On the other hand, Müller *et al*. show that the mixed modes are unstable, and only the longitudinal rolls and the transverse modes can be stable. This disagreement mainly comes from the difference of the coefficients of nonlinear interaction terms. Ouazzani *et al*. carried out experiments on this subject [15,16]. The aspect ratio of their channel was 3.63. The sidewalls of their apparatus are regarded to be insulating. Using water as the working fluid, they observed an irregular flow structure as well as longitudinal rolls and the transverse modes in the neighborhood of the crossover point.

In the present paper, without introducing any model, we derive amplitude equations governing the longitudinal rolls and the transverse modes for $(\mathrm{Re}, \mathrm{Ra}) \simeq (\mathrm{Re}_*, \mathrm{Ra}_*)$. Our derived equations are thus consistent with the fundamental equations of fluid motion in a rectangular channel. We determine the coefficients in the equations numerically. The amplitude equations have four equilibrium solutions; they exhibit the conduction state, longitudinal rolls, transverse modes, and mixed modes. We analyze the stability of each. We take account of both perfectly insulating and perfectly conducting sidewalls, to compare our results with the experimental results.

In Sec. II, we describe the fundamental equations of fluid motion, their steady solution corresponding to the conduction state, and equations for disturbance added to the steady solution. In Sec. III, we outline the linear stability characteristics with respect to the longitudinal rolls and transverse modes, and determine the crossover point, numerically. We derive the amplitude equations in Sec. IV, and predict stable patterns for given sets of parameters in Sec. V.

II. FORMULATION

We consider the motion of a Boussinesq fluid in an infinitely long horizontal channel. The cross section of the channel is a rectangle bounded by sidewalls at $y^* = \pm d/2$ and horizontal walls at $z^* = \pm h/2$. We apply a pressure gradient in the x^* direction in order to drive a through flow. The channel is heated from below and cooled from above at different but uniform temperatures $T^* = T_0 \mp \Delta T/2$ at $z^* = \pm h/2$. Here, T_0 is the reference temperature measured at $z^* = 0$, and ΔT (>0) is the temperature difference on the top and bottom walls. We introduce dimensionless variables, as usual, by a characteristic length h, a characteristic temperature ΔT, and a characteristic velocity U_0, which is equal to the maximum velocity of the basic flow. We denote the dimensionless variables by letters without an asterisk. We define the aspect ratio of the channel as $A = d/h$. The cross section of the channel is normalized as $|y| \leqslant A/2$ and $|z| \leqslant 1/2$. Pressure $p(\boldsymbol{x},t)$, velocity $\boldsymbol{u}(\boldsymbol{x},t) = (u(\boldsymbol{x},t), v(\boldsymbol{x},t), w(\boldsymbol{x},t))$, and temperature $T(\boldsymbol{x},t)$ of the fluid satisfy the following basic equations:

$$\boldsymbol{\nabla} \cdot \boldsymbol{u} = 0, \tag{1a}$$

$$\partial_t \boldsymbol{u} + (\boldsymbol{u} \cdot \boldsymbol{\nabla})\boldsymbol{u} = -\boldsymbol{\nabla}\pi + \mathrm{Ra}\,\mathrm{Pr}^{-1}\,\mathrm{Re}^{-2}[T - T_0/(\Delta T)]\hat{\boldsymbol{z}} + \mathrm{Re}^{-1}\boldsymbol{\nabla}^2\boldsymbol{u}, \tag{1b}$$

$$\partial_t T + (\boldsymbol{u} \cdot \boldsymbol{\nabla})T = \mathrm{Pr}^{-1}\,\mathrm{Re}^{-1}\boldsymbol{\nabla}^2 T, \tag{1c}$$

where $\pi = p + ghz/U_0^2$, g is the gravitational acceleration, and $\hat{\boldsymbol{z}}$ is a unit vector in the z direction. Equations (1) involve three nondimensional parameters. They are the Reynolds number Re, the Prandtl number Pr, and the Rayleigh number Ra defined by

$$\mathrm{Re} = hU_0/\nu, \quad \mathrm{Pr} = \nu/\kappa, \quad \mathrm{Ra} = \alpha \Delta T g h^3/(\nu\kappa).$$

Here, ν is the kinematic viscosity, κ is the thermal diffusivity, and α is the coefficient of cubical expansion. We impose the nonslip conditions $\boldsymbol{u} = \boldsymbol{0}$ on the rigid boundaries $y = \pm A/2$ and $z = \pm 1/2$. The temperatures on the top and bottom walls are $T = T_0/(\Delta T) \mp 1/2$ at $z = \pm 1/2$. The sidewalls at $y = \pm A/2$ are assumed to be perfectly conducting, satisfying $T = T_w(z)$, or perfectly insulating, satisfying $\partial_y T = 0$. Here, $T_w(z) = T_0/(\Delta T) - z$.

Consider the conduction state $(\overline{\Pi}, \overline{\boldsymbol{U}}, \overline{T})$ corresponding to the basic flow. The basic flow is steady, parallel, and uniform in the x direction. The temperature satisfying the boundary conditions is given by $\overline{T} = T_0/(\Delta T) - z$. The velocity $\overline{\boldsymbol{U}} = (\overline{U}(y,z), 0, 0)$ satisfies

$$(\partial_{yy} + \partial_{zz})\overline{U} = c, \tag{2}$$

where c on the right hand side is a negative constant proportional to the applied pressure gradient in the x direction. The constant c is chosen so that $\max \overline{U}(y,z) = 1$ holds. We impose the boundary conditions $\overline{U} = 0$ at $y = \pm A/2$ and $z = \pm 1/2$.

We expand $\overline{U}$ in Chebyshev polynomials.[1] The solution $\overline{U}$ is an even function of y and z, and is expanded as

[1] We may expand $\overline{U}$ in sinusoidal and hyperbolic functions, too. In this case, we have an analytical solution in an infinite series form. The Chebyshev expansion, however, gives a more accurate solution when we truncate the series at a finite level.

$$\overline{U}(y,z)=\sum_{m=0}^{M_U}\sum_{n=0}^{N_U} U_{mn}T_{2m}(2y/A)T_{2n}(2z), \tag{3}$$

where $T_n(x)$ is the Chebyshev polynomial of degree n. Substituting Eq. (3) into Eq. (2) and applying the tau collocation method, we obtain algebraic equations for the expansion coefficients U_{mn}. We solve them by the Newton-Raphson iteration. We correlate the truncation level M_U, N_U with the aspect ratio A of the cross section as $N_U = AM_U$. We set $M_U = 20$ for $A = 1.0, 2.0$, $M_U = 23$ for $A = 3.0$, and $M_U = 17$ for $A = 4.0$. Then, the expansion coefficients of the last terms in Eq. (3), $U_{M_U n}$ and U_{mN_U}, were of $O(10^{-6})$. The relative error in $\overline{U}$ was typically of $O(10^{-6})$. The influence of this error on the linear stability characteristics is small enough; it will be mentioned again in Sec. III B.

We now add a disturbance to the basic flow. We denote the disturbance components of pressure, velocity, and temperature as $\hat{\pi}(\boldsymbol{x},t)$, $\hat{\boldsymbol{u}}(\boldsymbol{x},t)=(\hat{u}(\boldsymbol{x},t),\hat{v}(\boldsymbol{x},t),\hat{w}(\boldsymbol{x},t))$, and $\hat{\theta}(\boldsymbol{x},t)$, respectively. Substituting $\pi=\overline{\Pi}+\hat{\pi}$, $\boldsymbol{u}=\overline{\boldsymbol{U}}+\hat{\boldsymbol{u}}$, and $\theta=\overline{T}+\hat{\theta}$ into Eq. (1) and subtracting the equations satisfied by $\overline{\Pi}$, $\overline{\boldsymbol{U}}$, and $\overline{T}$, we have the disturbance equations

$$\boldsymbol{\nabla}\cdot\hat{\boldsymbol{u}}=0, \tag{4a}$$

$$\partial_t\hat{\boldsymbol{u}}+(\overline{\boldsymbol{U}}\cdot\boldsymbol{\nabla})\hat{\boldsymbol{u}}+(\hat{\boldsymbol{u}}\cdot\boldsymbol{\nabla})\overline{\boldsymbol{U}}+(\hat{\boldsymbol{u}}\cdot\boldsymbol{\nabla})\hat{\boldsymbol{u}} = -\boldsymbol{\nabla}\hat{\pi}+\mathrm{Re}^{-1}\boldsymbol{\nabla}^2\hat{\boldsymbol{u}}+\mathrm{Ra}\,\mathrm{Pr}^{-1}\,\mathrm{Re}^{-2}\hat{\theta}\hat{\boldsymbol{z}}, \tag{4b}$$

$$\partial_t\hat{\theta}+\overline{U}\partial_x\hat{\theta}-\hat{w}+(\hat{\boldsymbol{u}}\cdot\boldsymbol{\nabla})\hat{\theta}=\mathrm{Pr}^{-1}\,\mathrm{Re}^{-1}\boldsymbol{\nabla}^2\hat{\theta}. \tag{4c}$$

Boundary conditions for the disturbance components are imposed as $\hat{\boldsymbol{u}}=\boldsymbol{0}$ and $\hat{\theta}=0$ at $z=\pm 1/2$, and $\hat{\boldsymbol{u}}=\boldsymbol{0}$ at $y=\pm A/2$. We impose $\hat{\theta}=0$ on the perfectly conducting sidewalls or $\partial_y\hat{\theta}=0$ on the perfectly insulating sidewalls at $y=\pm A/2$.

III. LINEAR STABILITY

In this section, we outline the linear stability characteristics of the basic flow with respect to the longitudinal rolls and transverse modes, and determine the crossover points numerically. Since the linear stability was studied in Refs. [7–11], as stated in Sec. I, we give only a brief outline in order to proceed to the weakly nonlinear analysis.

We consider an infinitesimal disturbance periodic in the x direction. We assume $\boldsymbol{\Phi}(\boldsymbol{x},t)\equiv(\hat{\pi}(\boldsymbol{x},t),\hat{\boldsymbol{u}}(\boldsymbol{x},t),\hat{\theta}(\boldsymbol{x},t))^{\mathrm{T}}$ in the normal mode,

$$\boldsymbol{\Phi}(\boldsymbol{x},t)=\boldsymbol{\phi}(y,z)\exp[i(kx-\omega t)], \tag{5}$$

with wave number k and complex frequency ω, where

$$\boldsymbol{\phi}(y,z)=(\tilde{\pi}(y,z),\tilde{\boldsymbol{u}}(y,z),\tilde{\theta}(y,z))^{\mathrm{T}}.$$

The imaginary part of ω is the growth rate of the disturbance. The disturbance with $k=0$ forms longitudinal rolls aligned along the x axis. The disturbance with $k\neq 0$ forms transverse modes, whose wave-number vector is parallel to the basic flow. The longitudinal rolls are two dimensional.

TABLE I. Parity of the linear eigenfunctions. The subscript e denotes an even function, and o an odd function. The function with eo, for instance, is even in the y direction and odd in the z direction.

Type of parity	Parity of disturbance
Parity 1	$(\tilde{p}_{eo},\tilde{u}_{eo},\tilde{v}_{oo},\tilde{w}_{ee},\tilde{\theta}_{ee})$
Parity 2	$(\tilde{p}_{oo},\tilde{u}_{oo},\tilde{v}_{eo},\tilde{w}_{oe},\tilde{\theta}_{oe})$
Parity 3	$(\tilde{p}_{ee},\tilde{u}_{ee},\tilde{v}_{oe},\tilde{w}_{eo},\tilde{\theta}_{eo})$
Parity 4	$(\tilde{p}_{oe},\tilde{u}_{oe},\tilde{v}_{ee},\tilde{w}_{oo},\tilde{\theta}_{oo})$

The transverse modes are three dimensional, since the sidewalls prevent a uniform motion in the spanwise direction.

Substituting Eq. (5) into Eq. (4) and linearizing the resultant equations, we have

$$\mathcal{L}_1\boldsymbol{\phi}=i\omega\mathcal{I}_1\boldsymbol{\phi}, \tag{6}$$

where $\mathcal{L}_1$ is an operator defined by

$$\mathcal{L}_n=\begin{pmatrix} 0 & nik & \partial_y & \partial_z & 0 \\ nik & \mathcal{S}_n^1 & \overline{U}_y & \overline{U}_z & 0 \\ \partial_y & 0 & \mathcal{S}_n^1 & 0 & 0 \\ \partial_z & 0 & 0 & \mathcal{S}_n^1 & -\mathrm{Ra}\,\mathrm{Pr}^{-1}\,\mathrm{Re}^{-2} \\ 0 & 0 & 0 & -1 & \mathcal{S}_n^2 \end{pmatrix} \quad (n=0,1,\ldots), \tag{7}$$

$$\mathcal{S}_n^1=nik\overline{U}-\mathrm{Re}^{-1}(\partial_{yy}+\partial_{zz}-n^2k^2),$$

$$\mathcal{S}_n^2=nik\overline{U}-\mathrm{Pr}^{-1}\,\mathrm{Re}^{-1}(\partial_{yy}+\partial_{zz}-n^2k^2).$$

The subscript y or z denotes the partial derivative with respect to itself. The operator $\mathcal{I}_1$ on the right hand side of Eq. (6) is a unit matrix whose diagonal component in the first row is replaced by zero. Equation (6) and the boundary conditions for $\boldsymbol{\phi}$ have reflection symmetries about the horizontal and vertical mid-planes of the channel. The symmetries enable us to classify the solutions into four classes with different parities. We call them parity 1, 2, 3, and 4 as defined in Table I.

A. Longitudinal rolls ($k=0$)

The eigenvalue ω is purely imaginary for the longitudinal rolls. Neutral stability ($\mathrm{Im}\,\omega=0$) therefore implies $\omega=0$, i.e., the principle of exchange of stabilities holds. The Rayleigh number giving neutral stability corresponds to the critical Rayleigh number. We denote it Ra_c^L. To find Ra_c^L, we substitute $k=0$ and $\omega=0$ into Eq. (6). The first equation of (6), coming from the equation of continuity (4a), allows us to introduce a stream function $\psi(y,z)$ such that $\tilde{v}=\psi_z/(\mathrm{Pr}\,\mathrm{Re})$ and $\tilde{w}=-\psi_y/(\mathrm{Pr}\,\mathrm{Re})$. Elimination of the pressure terms in Eq. (6) yields a closed form of equations for ψ and $\tilde{\theta}$:

$$(\partial_{yy}+\partial_{zz})^2\psi-\mathrm{Ra}_c^L\tilde{\theta}_y=0, \tag{8a}$$

$$(\partial_{yy}+\partial_{zz})\tilde{\theta}-\psi_y=0. \tag{8b}$$

TABLE II. Reynolds number Re_*, Rayleigh number Ra_*, wave number k_c, and frequency ω_c at the crossover point. The third column represents the parity of the longitudinal rolls. The transverse modes always have parity 1.

			Perfectly conducting sidewalls				Perfectly insulating sidewalls			
Pr	A	Parity	Re_*	Ra_*	k_c	ω_c	Re_*	Ra_*	k_c	ω_c
0.71	1.0	2	81.14	5011.71	2.55	1.72	16.61	2585.02	3.07	1.95
	2.0	1	37.46	2384.87	2.24	1.59	16.99	2013.21	2.74	1.96
	3.0	2	24.36	1996.28	2.70	2.00	16.74	1870.58	2.81	2.08
	4.0	1	18.42	1867.65	2.89	2.17	14.12	1810.27	2.94	2.20
7	1.0	2	14.00	5011.71	2.70	2.18	1.779	2585.02	3.13	2.17
	2.0	1	8.079	2384.87	2.14	1.79	3.335	2013.21	2.69	2.22
	3.0	2	5.317	1996.28	2.58	2.19	3.491	1870.58	2.74	2.32
	4.0	1	3.972	1867.65	2.80	2.40	2.993	1810.27	2.87	2.45

The boundary conditions are $\psi=\psi_z=\tilde{\theta}=0$ at $z=\pm 1/2$, and $\psi=\psi_y=0$ at $y=\pm A/2$. We impose $\tilde{\theta}=0$ on the perfectly conducting sidewalls or $\partial_y\tilde{\theta}=0$ on the perfectly insulating sidewalls at $y=\pm A/2$. The critical Rayleigh number Ra_c^L depends only on the aspect ratio, and is independent of the Reynolds number and the Prandtl number.

To solve Eq. (8) numerically, we expand ψ as

$$\psi(y,z)=\sum_{m=0}^{M}\sum_{n=0}^{N}\psi_{mn}F_m(2y/A)F_n(2z). \tag{9}$$

We expand $\tilde{\theta}$ as

$$\tilde{\theta}(y,z)=\sum_{m=0}^{M}\sum_{n=0}^{N}\theta_{mn}G_m(2y/A)G_n(2z) \tag{10}$$

for the perfectly conducting sidewalls, or as

$$\tilde{\theta}(y,z)=\sum_{m=0}^{M}\sum_{n=0}^{N}\theta_{mn}H_m(2y/A)G_n(2z) \tag{11}$$

for the perfectly insulating sidewalls. Here, the functions $F_n(x)$, $G_n(x)$, and $H_n(x)$ are defined by

$$F_{2n}(x)=T_{2n+4}(x)-(n+2)^2T_2(x)+(n+1)(n+3)T_0(x), \tag{12a}$$

$$F_{2n+1}(x)=T_{2n+5}(x)-\frac{1}{2}(n+2)(n+3)T_3(x)+\frac{1}{2}(n+1)(n+4)T_1(x), \tag{12b}$$

$$G_{2n}(x)=T_{2n+2}(x)-T_0(x), \tag{12c}$$

$$G_{2n+1}(x)=T_{2n+3}(x)-T_1(x), \tag{12d}$$

$$H_{2n}(x)=T_{2n+2}(x)-(n+1)^2T_2(x) \quad \text{for } n\neq 0, \tag{12e}$$

$$H_0(x)=T_0(x), \tag{12f}$$

$$H_{2n+1}(x)=T_{2n+3}(x)-(2n+3)^2T_1(x). \tag{12g}$$

They satisfy boundary conditions $F_n(\pm 1)=F_n'(\pm 1)=G_n(\pm 1)=H_n'(\pm 1)=0$. We substitute the expansions (9) and (10) [or (9) and (11)] into Eq. (8) and apply the collocation method. This yields a linear algebraic eigenvalue problem with eigenvalue Ra_c^L and eigenvector $(\psi_{00},\ldots,\psi_{MN},\theta_{00},\ldots,\theta_{MN})$. We solve the eigenvalue problem by the QZ method. Using the eigenvalue and eigenvector obtained as the initial guess, we make the solution more accurate by Newton-Raphson iteration. We adopted the truncation level $M=N=33$.

The critical Rayleigh number is shown in the column Ra_* in Table II. The table also involves stability information on transverse modes $(\mathrm{Re}_*,k_c,\omega_c)$; they have no direct relation to this subsection. The critical modes for $A=2.0$ and 4.0 have parity 1, and the modes for $A=1.0$ and 3.0 have parity 2. According to Refs. [10,11], the critical mode has parity 1 for $A\leqslant 1.6$, parity 2 for $1.6\leqslant A\leqslant 2.7$, parity 1 for $2.7\leqslant A\leqslant 3.7$, and so on. Our numerical data on Ra_c^L have ten significant figures, although we show only the first several figures in the table. They agree with the results of Ref. [10] based on the pseudospectral method[2] and the results of Ref. [11] based on the Galerkin method.

B. Transverse modes ($k\neq 0$)

Let us outline how to analyze the linear stability with respect to the transverse modes.

Elimination of $\tilde{\pi}$ and $\tilde{u}$ in $\boldsymbol{\phi}$ from Eq. (6) yields a closed form of equations for $\tilde{v},\tilde{w}$ and $\tilde{\theta}$:

$$\mathcal{T}_1(y,z)\tilde{v}+\mathcal{T}_2(y,z)\tilde{w}=i\omega[(\partial_{yy}-k^2)\tilde{v}+\partial_{yz}\tilde{w}], \tag{13a}$$

$$\mathcal{T}_2(z,y)\tilde{v}+\mathcal{T}_1(z,y)\tilde{w}+k^2\,\mathrm{Ra}\,\mathrm{Pr}^{-1}\,\mathrm{Re}^{-2}\tilde{\theta}=i\omega[\partial_{yz}\tilde{v}+(\partial_{zz}-k^2)\tilde{w}], \tag{13b}$$

[2] In Ref. [10], Lee *et al*. examined the pseudospectral method and the Galerkin method. The values of Ra_c^L by these methods converged to different values. They concluded that the latter method gave better accuracy. The validity of their ''less accurate'' results is confirmed by Ref. [11] and also by our computation. We also adopted the Galerkin method with the expansion (9)–(11), and obtained the same value of Ra_c^L as in Table II.

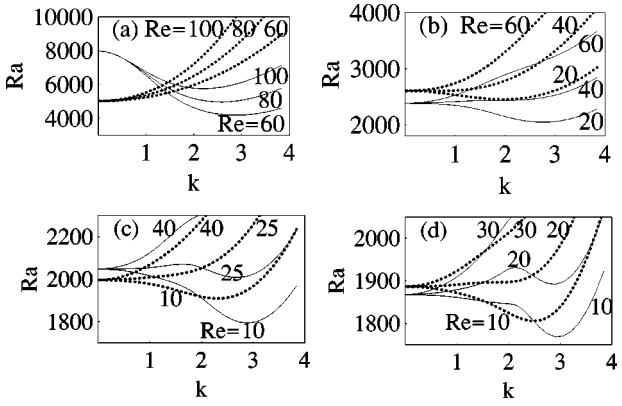

FIG. 1. The linear neutral stability curves for different values of Re. The solid lines represent the neutral curves for the transverse mode with parity 1, and the dotted lines denote the ones with parity 2. (a) $A=1.0$. (b) $A=2.0$. (c) $A=3.0$. (d) $A=4.0$. Pr = 0.71. Perfectly conducting sidewalls.

$$\mathcal{S}_1^2\tilde{\theta}-\tilde{w}=i\omega\tilde{\theta}, \tag{13c}$$

where

$$\mathcal{T}_1(y,z)=\mathcal{S}_1^1(\partial_{yy}-k^2)-ik\overline{U}_{yy},$$

$$\mathcal{T}_2(y,z)=\mathcal{S}_1^1\partial_{yz}+ik(\overline{U}_y\partial_z-\overline{U}_z\partial_y-\overline{U}_{yz}).$$

The operator $\mathcal{T}_n(z,y)$ is obtained by exchanging y and z in $\mathcal{T}_n(y,z)$ except for the arguments in $\overline{U}(y,z)$. The boundary conditions for the velocity are $\tilde{v}=\tilde{w}=\tilde{w}_z=0$ at $z=\pm 1/2$ and $\tilde{v}=\tilde{v}_y=\tilde{w}=0$ at $y=\pm A/2$. The boundary conditions for $\tilde{\theta}$ are the same as the conditions for the longitudinal rolls. We expand the amplitude functions of the normal mode, $\tilde{v}$ and $\tilde{w}$, so that they satisfy the boundary conditions

$$\tilde{v}(y,z)=\sum_{m=0}^{M}\sum_{n=0}^{N}v_{mn}F_m(2y/A)G_n(2z), \tag{14a}$$

$$\tilde{w}(y,z)=\sum_{m=0}^{M}\sum_{n=0}^{N}w_{mn}G_m(2y/A)F_n(2z). \tag{14b}$$

The functions $F_n(x)$ and $G_n(x)$ are defined by Eq. (12). Expansion of $\tilde{\theta}$ is given by Eq. (10) or Eq. (11), and is the same as that for the longitudinal rolls. We substitute Eqs. (10) and (14) [or Eqs. (11) and (14)] into Eq. (13), and apply the collocation method. We then obtain an algebraic eigenvalue problem with the eigenvalue ω for given values of A, Pr, Re, k, and Ra. We solve the eigenvalue problem by the QZ method. The accuracy of the numerical results was improved by means of the Newton-Raphson iteration under the constraint $\mathrm{Im}\,\omega=0$. We adopted the truncation level $M=N=33$. The accuracy of the linear stability characteristics may be affected by the numerical error in the basic flow $\overline{U}$. The relative error in ω due to the error in $\overline{U}$ was of $O(10^{-9})$; it resulted in an error in Re at the crossover points of $O(10^{-8})$.

Figure 1 shows the neutral curves for the transverse modes with parity 1 and 2, i.e., $(\tilde{p}_{eo},\tilde{u}_{eo},\tilde{v}_{oo},\tilde{w}_{ee},\tilde{\theta}_{ee})$ and $(\tilde{p}_{oo},\tilde{u}_{oo},\tilde{v}_{eo},\tilde{w}_{oe},\tilde{\theta}_{oe})$, respectively. The neutral Rayleigh numbers for modes with parity 3 and 4 are much greater than those for modes with parity 1 and 2. When a neutral curve has a local minimum, we call this the critical Rayleigh number for the transverse modes for a prescribed Re. We write it Ra_c^T. The corresponding wave number and frequency are denoted by k_c and ω_c, respectively.

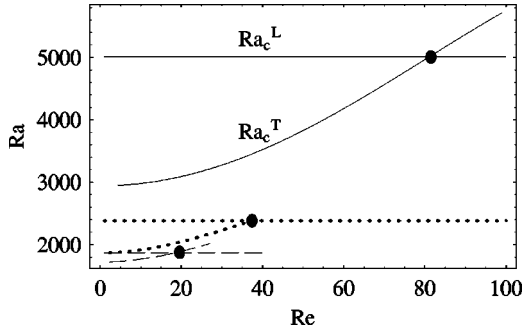

FIG. 2. The critical Rayleigh number as a function of the Reynolds number of the through flow. The solid lines represent Ra_c^L and Ra_c^T for $A=1$, the dotted lines are for $A=2$, and the dashed lines are for $A=4$. Pr = 0.71. Perfectly conducting sidewalls. The critical Rayleigh number Ra_c^L for longitudinal rolls is independent of Re. The closed circle denotes the crossover point, at which $\mathrm{Ra}_c^L=\mathrm{Ra}_c^T$ holds.

We calculated the critical conditions for a wide range of the Prandtl number, Pr = 0.001, 0.01, 0.1, 0.71, 1, 7, 10, 100, and 1000, for the aspect ratios $A=1.0$, 2.0, 3.0, and 4.0, and for perfectly conducting and insulating sidewalls. In all cases, except for Pr = 0.1 and $A=2.0$, Ra_c^T is an increasing function of Re as shown in Fig. 2.[3] The closed circles in the figure are the crossover points. At the crossover points, the critical Rayleigh number for the longitudinal rolls coincides with that for the transverse modes, that is, $\mathrm{Ra}_c^L=\mathrm{Ra}_c^T$ holds. We denote the crossover point by $(\mathrm{Re}_*,\mathrm{Ra}_*)$. For $\mathrm{Re}<\mathrm{Re}_*$, the transverse modes are critical, that is, $\mathrm{Ra}_c^T<\mathrm{Ra}_c^L$ holds. For $\mathrm{Re}>\mathrm{Re}_*$, the longitudinal rolls are critical, that is, $\mathrm{Ra}_c^L<\mathrm{Ra}_c^T$ holds. We omit the result for $A=3.0$ in Fig. 2 for clarity, since the value of Ra_c^T for $A=3.0$ is close to the one for $A=4.0$.

Table II summarizes the crossover point and corresponding parameters. We obtained Ra_* up to ten significant figures and Re_* to seven significant figures, although we show only the first several figures in the table. Our numerical data agree well with the data of Platten and Legros [7] for the insulating sidewalls, and with the data of Yamada *et al.* [8] for the conducting sidewalls.[4] Both Re_* and Ra_* are decreasing

[3]To our knowledge, it was Platten and Legros [7] who first illustrated the critical conditions in the Re-Ra plane and obtained the crossover point for several parameters under insulating sidewall conditions. Later, Yamada *et al.* [8] made a similar plot for the perfectly conducting situation.

[4]Yamada *et al.* determined the crossover point by using Ra_c^L in Refs. [10] and [11]. The values of Ra_c^L calculated by the Galerkin method in Ref. [10] disagree with those in Ref. [11]; Yamada *et al.* showed two kinds of crossover point based on the different values of Ra_c^L. Our crossover points agree with their data based on Ra_c^L in Ref. [11].

TABLE III. Coefficients in the amplitude equations under perfectly conducting sidewall conditions. The superscript r denotes the real part of the attached quantity.

Pr	A	$\lambda_{0\mathrm{Ra}}$	$\lambda^r_{1\mathrm{Re}}$	$\lambda^r_{1\mathrm{Ra}}$	λ_{000}	λ_{110}	λ^r_{111}	λ^r_{001}
0.71	1.0	-0.752309×10^{-4}	-20.110	-0.75398×10^{-4}	0.110272	5.445	2.206	0.1209
	2.0	-2.134152×10^{-4}	-6.3972	-2.2157×10^{-4}	1.453285	3.589	1.566	3.804
	3.0	-3.576159×10^{-4}	-3.98138	-3.6702×10^{-4}	0.1812198	2.353	2.299	0.3933
	4.0	-4.891387×10^{-4}	-2.4984	-4.9875×10^{-4}	2.357924	4.021	3.027	4.817
7	1.0	-0.8940293×10^{-4}	-3.660	-0.87713×10^{-4}	0.120587	1.788	1.759	0.1348
	2.0	-1.656756×10^{-4}	-0.92208	-1.6966×10^{-4}	1.087214	1.385	0.8465	2.417
	3.0	-2.695566×10^{-4}	-0.598330	-2.7548×10^{-4}	0.1343626	1.094	1.1887	0.2063
	4.0	-3.712467×10^{-4}	-0.387217	-3.7786×10^{-4}	1.762920	1.639	1.611	2.950

functions of the aspect ratio for perfectly conducting sidewalls. They are not, however, for insulating sidewalls.

IV. WEAKLY NONLINEAR REDUCTION TO THE AMPLITUDE EQUATIONS

Except for the neighborhood of the crossover point, the linear stability theory well predicts the convection pattern due to primary bifurcation. In that neighborhood, the linear theory loses its validity, since nonlinear interaction plays a significant role in the pattern formation. In the following sections, we focus on the interaction between the longitudinal rolls and transverse modes. In this section, we derive amplitude equations governing the temporal evolution of these modes.

Our weakly nonlinear reduction is based on a perturbation expansion about the crossover point $(\mathrm{Re}_*,\mathrm{Ra}_*)$. We introduce a small parameter ϵ defined by

$$\epsilon^2=\frac{1}{\mathrm{Re}_*}-\frac{1}{\mathrm{Re}}$$

and set

$$\mathrm{Ra}=\mathrm{Ra}_*+\epsilon^2\tilde{R}$$

where $\tilde{R}=O(1)$. Exactly at the crossover point ($\epsilon=0$), the dominant modes are the critical longitudinal rolls with $k=0$ and the critical transverse modes with $k=k_c$ ($\neq0$). All the other modes decay on a linear basis. Nonlinear interaction between the dominant modes excites their higher harmonics. Assuming $\|\mathbf{\Phi}\|=O(\epsilon)$, we expand the disturbance $\mathbf{\Phi}$ as

$$\mathbf{\Phi}=\sum_{n=-\infty}^{\infty}\sum_{m=\max(1,|n|)}^{\infty}\epsilon^m\mathbf{\Phi}_{nm}\exp[ni(k_cx-\omega_ct)]. \quad (15)$$

For $\mathbf{\Phi}$ to be real, we require $\mathbf{\Phi}_{-nm}=\mathbf{\Phi}^*_{nm}$ for $n\geqslant1$, where the asterisk denotes the complex conjugate. Note that $\mathbf{\Phi}_{0m}$ is real. We assume that the amplitudes $\mathbf{\Phi}_{nm}$ vary slowly in time, compared with the time scale of $O(\omega_c^{-1})$. Introducing multiple time scales $t_k=\epsilon^{2k}t$ for $k=1,2,\ldots$, we set $\mathbf{\Phi}_{nm}=\mathbf{\Phi}_{nm}(y,z,t_1,t_2,\ldots)$. We ignore spatial modulations of the amplitudes throughout.

We now expand the disturbance equations (4) about the crossover point $(\mathrm{Re}_*,\mathrm{Ra}_*)$, and substitute Eq. (15) into the resultant equations. At $O(\epsilon)$, we have

$$(-ni\omega_c\mathcal{I}_1+\mathcal{L}_n)\mathbf{\Phi}_{n1}=\mathbf{0} \quad \text{for } n=0,1. \quad (16)$$

In what follows, we set $(k,\mathrm{Re},\mathrm{Ra})=(k_c,\mathrm{Re}_*,\mathrm{Ra}_*)$ in the operators (7). Since the operators in Eq. (16) are independent of time, the solution is written as

$$\mathbf{\Phi}_{n1}=A_{n1}(t_1,t_2,\ldots)\boldsymbol{\phi}_{n1}(y,z) \quad \text{for } n=0,1.$$

The function $\boldsymbol{\phi}_{n1}=(\pi_{n1},\boldsymbol{u}_{n1},\theta_{n1})^{\mathrm{T}}$ is the linear eigenfunction of the longitudinal rolls for $n=0$ and the transverse modes for $n=1$. The eigenfunction is indeterminate by a multiple. To obtain a unique function, we normalize $\boldsymbol{\phi}_{n1}$ such that $\theta_{n1}(0,0)=1$ for modes with parity 1 or $\partial_y\theta_{n1}(0,0)=1$ for parity 2.

At $O(\epsilon^2)$, we have

$$(-ni\omega_c\mathcal{I}_1+\mathcal{L}_n)\mathbf{\Phi}_{n2}=N_{n2} \quad \text{for } n=0,1,2. \quad (17)$$

The nonlinear term N_{n2} consists of $\boldsymbol{\phi}_{01}$ and $\boldsymbol{\phi}_{11}$. For its explicit form, see the Appendix. We can write the solution as

$$\mathbf{\Phi}_{02}=A_{02}\boldsymbol{\phi}_{01}+(A_{01})^2\boldsymbol{\phi}^{00}_{02}+|A_{11}|^2\boldsymbol{\phi}^{11}_{02},$$

$$\mathbf{\Phi}_{12}=A_{12}\boldsymbol{\phi}_{11}+A_{01}A_{11}\boldsymbol{\phi}^{01}_{12},$$

$$\mathbf{\Phi}_{22}=(A_{11})^2\boldsymbol{\phi}^{11}_{22}$$

where $\boldsymbol{\phi}^{pq}_{nm}$ is a function of y and z and is obtained numerically. New amplitude functions A_{02} and A_{12} of $t_1,t_2,\ldots$ arise at this order of approximation.

At $O(\epsilon^3)$, we have

$$(-ni\omega_c\mathcal{I}_1+\mathcal{L}_n)\mathbf{\Phi}_{n3}=N_{n3} \quad \text{for } n=0,1. \quad (18)$$

The term N_{n3} on the right hand side is given in the Appendix. A solution of Eq. (18) exists only if N_{n3} satisfies the solvability condition, i.e., only if N_{n3} is orthogonal to the solution of the adjoint problem.[5] The adjoint problem is written as $(ni\omega_c\mathcal{I}_1+\mathcal{L}^\dagger_n)\boldsymbol{\phi}^\dagger_n=0$, subject to appropriate boundary conditions. Here, the operator $\mathcal{L}^\dagger_n$ satisfies

$$\langle(-ni\omega_c\mathcal{I}_1+\mathcal{L}_n)\boldsymbol{\psi}_1,\boldsymbol{\psi}_2\rangle=\langle\boldsymbol{\psi}_1,(ni\omega_c\mathcal{I}_1+\mathcal{L}^\dagger_n)\boldsymbol{\psi}_2\rangle$$

[5]The solvability condition for Eq. (17) is satisfied without any extra condition, since N_{n2} has a different parity from the parity of the adjoint function.

for arbitrary functions $\boldsymbol{\psi}_1, \boldsymbol{\psi}_2$ satisfying the boundary conditions. The angular bracket denotes the inner product defined by

$$\langle \boldsymbol{\psi}_1, \boldsymbol{\psi}_2 \rangle \equiv \int_{-1/2}^{1/2} \int_{-A/2}^{A/2} \boldsymbol{\psi}_1 \cdot \boldsymbol{\psi}_2^* dy dz. \tag{19}$$

The explicit form of $\mathcal{L}_n^\dagger$ is

$$\mathcal{L}_n^\dagger = \begin{pmatrix} 0 & -nik_c & -\partial_y & -\partial_z & 0 \\ -nik_c & \mathcal{S}_{-n}^1 & 0 & 0 & 0 \\ -\partial_y & \overline{U}_y & \mathcal{S}_{-n}^1 & 0 & 0 \\ -\partial_z & \overline{U}_z & 0 & \mathcal{S}_{-n}^1 & -1 \\ 0 & 0 & 0 & -\mathrm{Ra}_* \, \mathrm{Pr}^{-1} (\mathrm{Re}_*)^{-2} & \mathcal{S}_{-n}^2 \end{pmatrix}.$$

When we write $\boldsymbol{\phi}_n^\dagger = (\pi_n^\dagger, \boldsymbol{u}_n^\dagger, \theta_n^\dagger)^{\mathrm{T}}$, the boundary conditions are given by $\boldsymbol{u}_n^\dagger = \mathbf{0}$ at $y = \pm A/2$ and $z = \pm 1/2$, and $\theta_n^\dagger = 0$ at $z = \pm 1/2$. We have $\theta_n^\dagger = 0$ on the perfectly conducting sidewalls or $\partial_y \theta_n^\dagger = 0$ on the perfectly insulating sidewalls at $y = \pm A/2$.

Finally, we define the amplitudes of the temperature disturbance at the center of the channel as $A_L = \epsilon A_{01} + \epsilon^2 A_{02} + \cdots$ and $A_T = \epsilon A_{11} + \epsilon^2 A_{12} + \cdots$, and use the original time scale t. Two solvability conditions for Eq. (18) yield the amplitude equations for A_L and A_T:

$$\frac{dA_L}{dt} + \epsilon^2 \tilde{R} \lambda_{0\,\mathrm{Ra}} A_L + \lambda_{000} (A_L)^3 + \lambda_{110} |A_T|^2 A_L + \cdots = 0, \tag{20a}$$

$$\frac{dA_T}{dt} + \epsilon^2 (-\lambda_{1\,\mathrm{Re}} + \tilde{R} \lambda_{1\,\mathrm{Ra}}) A_T + \lambda_{111} |A_T|^2 A_T + \lambda_{001} (A_L)^2 A_T + \cdots = 0. \tag{20b}$$

The amplitude A_L is a real function, and the coefficients in Eq. (20a) are real. The amplitude A_T and the coefficients in Eq. (20b) are complex. Tables III and IV show the coefficients for several values of Pr and A. We do not list the imaginary parts of the coefficients, since they are not necessary to examine convection patterns in the next section.

For simplicity of the analysis, we neglected the spatial dependence of A_L and A_T entirely. If we allow spatiotemporal dependence, we get coupled envelope equations, instead of Eqs. (20). They are similar to the equations in Refs. [13] and [14]. The coefficients of nonlinear terms in this case are exactly the same as the ones in Eqs. (20).

V. CONVECTION PATTERNS

We analyze the nonlinear interaction at the lowest order described by the cubic terms in Eqs. (20). We set $A_L(t) = a(t)$ and $A_T(t) = b(t) \exp[i\rho(t)]$, where the amplitudes $a(t), b(t)$ and the phase $\rho(t)$ are real functions. Then we have

$$\frac{da}{dt} + (-\lambda_0 + \lambda_{000} a^2 + \lambda_{110} b^2) a = 0, \tag{21a}$$

$$\frac{db}{dt} + (-\lambda_1^r + \lambda_{111}^r b^2 + \lambda_{001}^r a^2) b = 0, \tag{21b}$$

where $\lambda_0 = -\epsilon^2 \tilde{R} \lambda_{0\,\mathrm{Ra}}$ and $\lambda_1^r = \epsilon^2 (\lambda_{1\,\mathrm{Re}}^r - \tilde{R} \lambda_{1\,\mathrm{Ra}}^r)$. The superscript r denotes the real part of the attached quantity. The coefficients λ_0 and λ_1^r, respectively, represent the linear growth rates of the longitudinal rolls and the transverse modes at $(\mathrm{Re}, \mathrm{Ra}) \simeq (\mathrm{Re}_*, \mathrm{Ra}_*)$. While the phase $\rho(t)$ depends on the amplitudes, the amplitudes $a(t)$ and $b(t)$ are independent of the phase. We therefore omit the equation for $\rho(t)$, for the phase itself has little role in pattern selection.

In this section, we obtain the equilibrium solutions of Eq. (21), examine their stability, and specify stable convection patterns. Since the generalized equations of (21) are analyzed in detail in Ref. [17], we mainly describe the stability of the mixed modes. Equations (21) are invariant under the transformation $a \to -a$ and $b \to -b$. We confine ourselves to the solutions with positive a and b.

TABLE IV. Coefficients in the amplitude equations under the perfectly insulating sidewall conditions.

Pr	A	$\lambda_{0\mathrm{Ra}}$	$\lambda_{1\mathrm{Re}}^r$	$\lambda_{1\mathrm{Ra}}^r$	λ_{000}	λ_{110}	λ_{111}^r	λ_{001}^r
0.71	1.0	-4.390980×10^{-4}	-3.14	$-4.4826278 \times 10^{-4}$	0.28215649	10.03	8.048	0.410372
	2.0	$-5.1106572 \times 10^{-4}$	-2.06671	$-5.3015167 \times 10^{-4}$	3.1294303	5.8624	3.8104	7.52125792
	3.0	$-5.4371806 \times 10^{-4}$	-2.13913	-5.467975×10^{-4}	0.257608870	3.82753	3.847184	0.55317991
	4.0	-6.560997×10^{-4}	-1.58386	$-6.5597676 \times 10^{-4}$	3.1500921	5.2752	4.599	6.464147
7	1.0	-6.057652×10^{-4}	-0.502	$-6.8593758 \times 10^{-4}$	0.3862774	6.14	6.598	0.487160
	2.0	$-4.1337049 \times 10^{-4}$	-0.30716	$-4.5202766 \times 10^{-4}$	2.49173560	2.4592	2.0646	5.2725882
	3.0	$-4.21691450 \times 10^{-4}$	-0.3240945	$-4.2995333 \times 10^{-4}$	0.19689802	1.60487	1.904613	0.31546536
	4.0	-5.038431×10^{-4}	-0.2418145	$-5.0561005 \times 10^{-4}$	2.3847966	1.967257	2.2498	3.88803

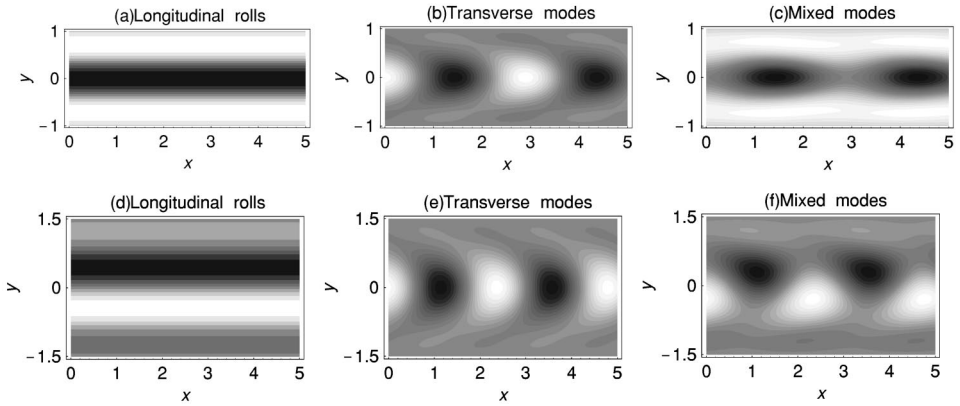

FIG. 3. Planform of the temperature disturbance on the horizontal mid-plane $z=0$. The lighter shades are hot and the darker shades are cold. (a), (d) Longitudinal rolls; (b), (e) transverse modes; (c), (f) the mixed modes with $D_a/D_b=7/3$. (a)–(c) $A=2.0$, (b)–(d) $A=3.0$. Pr = 7. Perfectly conducting sidewalls.

We call the solution equilibrium if a and b are time independent. The trivial solution $a=b=0$ represents the conduction state. In addition to it, we have the following nontrivial equilibrium solutions: (i) longitudinal rolls, $a=\sqrt{\lambda_0/\lambda_{000}}$, $b=0$, (ii) transverse modes, $a=0$, $b=\sqrt{\lambda_1^r/\lambda_{111}^r}$, and (iii) mixed modes, $a=\sqrt{D_a/D}$, $b=\sqrt{D_b/D}$, where $D_a=\lambda_{110}\lambda_1^r-\lambda_0\lambda_{111}^r$, $D_b=\lambda_0\lambda_{001}^r-\lambda_{000}\lambda_1^r$, and $D=\lambda_{110}\lambda_{001}^r-\lambda_{000}\lambda_{111}^r$. Figure 3 demonstrates typical convection patterns exhibited by these solutions. While the longitudinal rolls exhibit steady patterns, the transverse and mixed modes exhibit traveling patterns. The patterns of the mixed modes depend on the value of D_a/D_b. Figures 3(c) and 3(f) show the patterns for $D_a/D_b=7/3$.

The equilibrium solutions vary their bifurcation characteristics depending on the signs of the nonlinear coefficients. We classify the combinations of the cubic coefficients into four types (type 1–type 4) as shown in Table V. According to our numerical results, the coefficients λ_{000} and λ_{110} are positive irrespective of the values of Pr and A in all the cases examined. From the definition of D, we have $D<0$ for type 2 and $D>0$ for type 3. For types 1 and 4, the sign of D is due to our numerical values of coefficients. We obtain $D>0$ for type 1 and $D<0$ for type 4 in all cases. For Pr $=0.71$, 1, 7, 10, 100, 1000 and $A=1.0$, 2.0, 3.0, 4.0, the coefficients belong to type 1. For Pr $\leqslant 0.1$, the nonlinear interaction varies in type as shown in Table VI. For Pr $=0.1$ and $A=2.0$, we have not found the crossover point.

Longitudinal rolls exist in the region $\mathrm{Ra}>\mathrm{Ra}_*$, since the coefficient $\lambda_{0\,\mathrm{Ra}}$ is negative. (See Tables III and IV.) Since λ_{000} is positive, the longitudinal rolls are stable in the absence of transverse components; in other words, they bifurcate supercritically. The transverse modes exist where λ_1^r has the same sign as λ_{111}^r. For types 1 and 2 ($\lambda_{111}^r>0$), they exist in the region $\lambda_1^r>0$, or equivalently, $\lambda_{1\,\mathrm{Re}}^r(1/\mathrm{Re}_*-1/\mathrm{Re})<\lambda_{1\,\mathrm{Ra}}^r(\mathrm{Ra}-\mathrm{Ra}_*)$. Their bifurcation is supercritical. For types 3 and 4 ($\lambda_{111}^r<0$), the bifurcation is subcritical, that is to say, the transverse modes are unstable even if the disturbance does not include a longitudinal component. In Fig. 4, the equilibrium solutions for all the types are classified in the Re-Ra plane.

Now, we examine the stability of the equilibrium solutions. First, we look into the type 1 solution in detail. Figures 5(a)–5(e) show the trajectories of the solutions of Eqs. (21) belonging to type 1. Locally, all the trajectories approach stable equilibrium solutions as $t\to\infty$. In Fig. 5(e), the trajectories approach the longitudinal rolls or the transverse modes, according to their initial values. We summarize the stability of the equilibrium solutions for type 1 in Fig. 4(a). We find at least one stable equilibrium solution, including the trivial one, in an arbitrary neighborhood of the crossover point. The mixed mode solution is unstable in any neighborhood of $(\mathrm{Re}_*,\mathrm{Ra}_*)$.

For all the cases belonging to type 1, our numerical computation results in positive D. Let us set D negative. The trajectories in regions a–d of Fig. 4 remain the same as in Figs. 5(a)–5(d) for positive D. The trajectory in region e, however, behaves as in Fig. 5(f) instead of Fig. 5(e). The mixed mode solution becomes stable. As above, the sign of D determines the stability of the mixed mode solution belonging to type 1. In previous studies [13] and [14], the coefficients in the envelope equations belong to type 1. Brand *et al.* examined the cases of positive and negative D, and found stable mixed mode patterns for negative D [13]. Müller *et al.* obtained positive D in their analysis [14].

Next, we turn to types 2, 3, and 4. Figures 5(g)–5(l) demonstrate the trajectories in the sectors g–ℓ in Figs. 4(b)–4(d), where mixed modes exist. The mixed modes are stable for type 2 and unstable for type 3. For type 4, the stability of the mixed modes depends on the value of (Re,Ra). The mixed modes are stable in the region k of Fig. 4, where $\sigma\equiv-(\lambda_{000}D_a+\lambda_{111}^rD_b)/D$ is negative. They are unstable in the region ℓ, where σ is positive. When $\sigma=0$, the mixed modes are neutral, and periodic solutions appear as shown in Fig. 5(m). Figure 4 summarizes the stability of all the equilibrium solutions for four types of cubic coefficients given in Table V.

When the transverse modes bifurcate subcritically [types 3 and 4, Figs. 5(i)–5(m)], some solutions diverge to infinity

TABLE V. Four types of the combination of signs of the nonlinear coefficients, and the sign of $D=\lambda_{110}\lambda_{001}^r-\lambda_{000}\lambda_{111}^r$. The sign of D for types 2 and 3 is due to the sign of λ_{000}, λ_{110}, λ_{111}^r, and λ_{001}^r. The sign of D for types 1 and 4 is due to the numerical values of the coefficients.

	λ_{000}	λ_{110}	λ_{111}^r	λ_{001}^r	D
Type 1	+	+	+	+	+
Type 2	+	+	+	−	−
Type 3	+	+	−	+	+
Type 4	+	+	−	−	−

TABLE VI. Type of the nonlinear coefficients for Pr $\leqslant 0.1$. We have not found the crossover point for Pr = 0.1 and $A=2$.

Pr	A	Conducting sidewalls	Insulating sidewalls
0.1	1.0	type 2	type 2
	2.0	—	—
	3.0	3	1
	4.0	3	3
0.01	1.0	2	4
	2.0	3	1
	3.0	3	3
	4.0	3	3
0.001	1.0	2	4
	2.0	3	1
	3.0	3	3
	4.0	3	3

$b\rightarrow\infty$, according to the cubic amplitude equations (21). This suggests another stable equilibrium solution with much larger amplitude. To resolve such a strongly nonlinear solution, the range of validity of the amplitude equations is too narrow; fully numerical analysis is necessary. This is beyond the scope of our paper.

Let us now compare our results with experimental results. Ouazzani *et al*. [15] studied convection patterns, using a water channel (Pr=7) with the aspect ratio 3.63. They carried out pointwise measurement of the vertical velocity by means of laser Doppler anemometry. They classified the patterns in five categories in their Fig. 18: the thermal conduction state, longitudinal rolls, transverse modes, longitudinal rolls or transverse modes (depending on the initial state), and an irregular flow. In our analysis, all the nonlinear coefficients have positive real parts for Pr=7 and $A=3.0,4.0$, for both conducting and insulating sidewalls (see Tables III and IV). The coefficients relevant to their experiment thus belong to type 1. The stable (therefore experimentally observable) patterns in Fig. 4(a) agree with the observed patterns classified in Ref. [15], except for the irregular flow. The present analysis is thus valid to predict actual convection patterns in laboratory experiments in the neighborhood of the crossover point, to some extent.

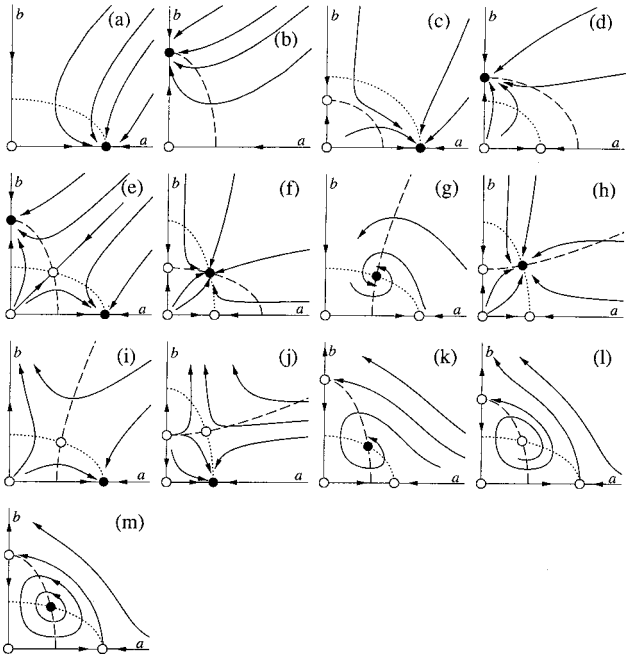

FIG. 5. Trajectories of solutions of Eqs. (21) in a-b plane. The figures (a)–(e), (g)–(l), respectively, represent the trajectories in the regions a–e, g–ℓ in Fig. 4. The figure (f) represents the trajectories in the region e in the case of $D<0$, and (m) shows the trajectories for $\sigma=0$ and type 4. The closed circle denotes the stable equilibrium solution and the open circle denotes the unstable one. The dotted line denotes $da/dt=0$, and the dashed line denotes $db/dt=0$.

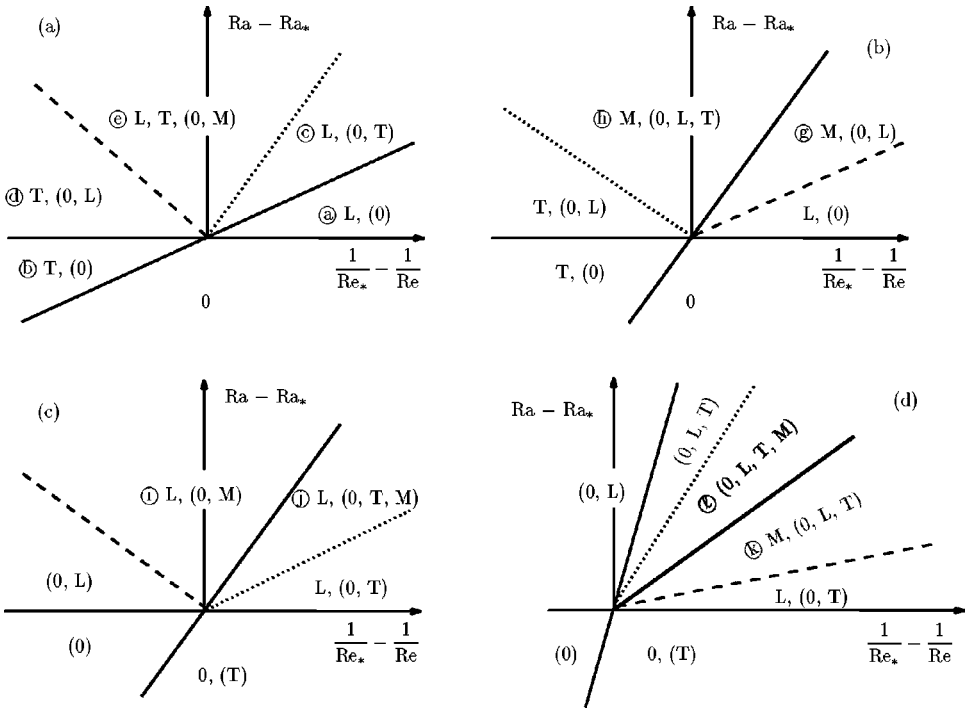

FIG. 4. Stability diagrams in $(\mathrm{Ra}-\mathrm{Ra}_*, 1/\mathrm{Re}_*-1/\mathrm{Re})$ plane. (a) Type 1 with positive D, (b) type 2 ($D<0$), (c) type 3 ($D>0$), and (d) type 4 with negative D. 0 denotes the trivial solution, L denotes the longitudinal rolls, T denotes the transverse modes, and M denotes the mixed mode. 0, L, T, M without parentheses denotes the stable solution, whereas with parentheses it denotes the unstable solution. The solid line denotes $\lambda_1^r=0$, the dotted line denotes $D_a=0$, the dashed line denotes $D_b=0$. The bold solid line in (d) denotes $\sigma\equiv-(\lambda_{000}D_a+\lambda_{111}^r D_b)/D=0$.

The only difference between our results and the experimental ones is the existence of the irregular flow. Ouazzani *et al*. observed a flow structure irregular in time. The irregular flow involved the longitudinal and transverse components. They did not mention whether the irregularity is spatiotemporal. The present analysis did not yield an irregular solution; neither did the analyses of the envelope equations [13,14]. To explain the irregular flow, we seem to need to take account of more complex interaction. Remember that the critical longitudinal rolls change their parity at $A=3.7$ on the linear basis [10,11]. The eigenfunction of the least stable mode exhibits three rolls (parity 2) for $A<3.7$ and four rolls (parity 1) for $A>3.7$. The aspect ratio of the channel in the experiment is 3.63 and agrees with the value of 3.7. In fact, Ouazzani *et al*. reported that four rolls almost always existed, and three rolls sometimes did in the parameter range where the longitudinal rolls exist stably. This supports the fact that the critical Rayleigh numbers are close together for three and four longitudinal rolls. In such a case, the interaction between two kinds of longitudinal rolls becomes important, in addition to the interaction between the longitudinal rolls and the transverse modes. We have neglected the former interaction in this paper. We hope that the amplitude/envelope equations describing the three-mode interaction will explain the experimentally observed irregular flow. Analysis of the three-mode interaction is in progress and will be reported elsewhere.

ACKNOWLEDGMENT

The authors gratefully acknowledge the support of the Advanced Science Research Center of the Japan Atomic Energy Research Institute.

APPENDIX: THE FUNCTIONS IN EQS. (17) AND (18) AND THE COEFFICIENTS IN EQS. (20)

We define a vector and an operator:

$$\boldsymbol{\phi}_{nm}=(\pi_{nm},\boldsymbol{u}_{nm},\theta_{nm})^{\mathrm{T}},$$

$$N(\boldsymbol{\phi}_{nm},\boldsymbol{\phi}_{pq})=(pik_c u_{nm}+v_{nm}\partial_y+w_{nm}\partial_z)\boldsymbol{\phi}_{pq},$$

$$N(\boldsymbol{\phi}_{nm},\boldsymbol{\phi}^*_{pq})=(-pik_c u_{nm}+v_{nm}\partial_y+w_{nm}\partial_z)\boldsymbol{\phi}^*_{pq},$$

$$N(\boldsymbol{\phi}^*_{nm},\boldsymbol{\phi}_{pq})=(pik_c u^*_{nm}+v^*_{nm}\partial_y+w^*_{nm}\partial_z)\boldsymbol{\phi}_{pq},$$

where the asterisk denotes the complex conjugate of the attached quantity.

The nonlinear terms in Eq. (17) are as follows:

$$N_{02}=-[(A_{01})^2N(\boldsymbol{\phi}_{01},\boldsymbol{\phi}_{01})+2|A_{11}|^2N(\boldsymbol{\phi}_{11},\boldsymbol{\phi}^*_{11})],$$

$$N_{12}=-A_{01}A_{11}[N(\boldsymbol{\phi}_{01},\boldsymbol{\phi}_{11})+N(\boldsymbol{\phi}_{11},\boldsymbol{\phi}_{01})],$$

$$N_{22}=-(A_{11})^2N(\boldsymbol{\phi}_{11},\boldsymbol{\phi}_{11}).$$

The terms N_{n3} on the right hand side of Eq. (18) are as follows:

$$\begin{aligned}N_{03}=-[&\partial_{t_1}A_{01}\mathcal{I}_1\boldsymbol{\phi}_{01}+A_{01}(-\mathcal{L}_{0\mathrm{Re}}+\tilde{R}\mathcal{L}_{0\mathrm{Ra}})\boldsymbol{\phi}_{01}\\&+2A_{01}A_{02}N(\boldsymbol{\phi}_{01},\boldsymbol{\phi}_{01})+2(A_{11}A^*_{12}\\&+A_{12}A^*_{11})N(\boldsymbol{\phi}_{11},\boldsymbol{\phi}^*_{11})+(A_{01})^3M_{000}+|A_{11}|^2A_{01}M_{110}],\end{aligned}$$

$$\begin{aligned}N_{13}=-\{&\partial_{t_1}A_{11}\mathcal{I}_1\boldsymbol{\phi}_{11}+A_{11}(-\mathcal{L}_{1\mathrm{Re}}+\tilde{R}\mathcal{L}_{1\mathrm{Ra}})\boldsymbol{\phi}_{11}\\&+(A_{01}A_{12}+A_{02}A_{11})[N(\boldsymbol{\phi}_{01},\boldsymbol{\phi}_{11})+N(\boldsymbol{\phi}_{11},\boldsymbol{\phi}_{01})]\\&+(A_{01})^2A_{11}M_{001}+|A_{11}|^2A_{11}M_{111}\},\end{aligned}$$

where

$$M_{000}=N(\boldsymbol{\phi}_{01},\boldsymbol{\phi}^{00}_{02})+N(\boldsymbol{\phi}^{00}_{02},\boldsymbol{\phi}_{01}),$$

$$\begin{aligned}M_{110}=&N(\boldsymbol{\phi}_{01},\boldsymbol{\phi}^{11}_{02})+N(\boldsymbol{\phi}^{11}_{02},\boldsymbol{\phi}_{01})+2N(\boldsymbol{\phi}_{11},(\boldsymbol{\phi}^{01}_{12})^*)\\&+2N(\boldsymbol{\phi}^{01}_{12},\boldsymbol{\phi}^*_{11}),\end{aligned}$$

$$\begin{aligned}M_{001}=&N(\boldsymbol{\phi}_{01},\boldsymbol{\phi}^{01}_{12})+N(\boldsymbol{\phi}^{01}_{12},\boldsymbol{\phi}_{01})+N(\boldsymbol{\phi}_{11},\boldsymbol{\phi}^{00}_{02})\\&+N(\boldsymbol{\phi}^{00}_{02},\boldsymbol{\phi}_{11}),\end{aligned}$$

$$\begin{aligned}M_{111}=&N(\boldsymbol{\phi}_{11},\boldsymbol{\phi}^{11}_{02})+N(\boldsymbol{\phi}^{11}_{02},\boldsymbol{\phi}_{11})+N(\boldsymbol{\phi}^*_{11},\boldsymbol{\phi}^{11}_{22})\\&+N(\boldsymbol{\phi}^{11}_{22},\boldsymbol{\phi}^*_{11}).\end{aligned}$$

The operators $\mathcal{L}_{n\,\mathrm{Re}}$ and $\mathcal{L}_{n\,\mathrm{Ra}}$ are defined by

$$\mathcal{L}_{n\,\mathrm{Re}}=\frac{\partial\mathcal{L}_n}{\partial(\mathrm{Re}_*^{-1})},\quad \mathcal{L}_{n\,\mathrm{Ra}}=\frac{\partial\mathcal{L}_n}{\partial\,\mathrm{Ra}_*},$$

where the operator $\mathcal{L}_n$ is given by Eq. (7).

The coefficients in Eqs. (20) are

$$\lambda_{n\,\mathrm{Re}}=\langle\mathcal{L}_{n\,\mathrm{Re}}\boldsymbol{\phi}_{n1}\rangle_n,\quad \lambda_{n\,\mathrm{Ra}}=\langle\mathcal{L}_{n\,\mathrm{Ra}}\boldsymbol{\phi}_{n1}\rangle_n,$$

$$\lambda_{ijk}=\langle M_{ijk}\rangle_k.$$

The angular bracket with the subscript 0 or 1 denotes the operation

$$\langle\cdot\rangle_n=\frac{\langle\cdot,\boldsymbol{\phi}^\dagger_n\rangle}{\langle\boldsymbol{\phi}_{n1},\boldsymbol{\phi}^\dagger_n\rangle}\quad(n=0,1)$$

where $\boldsymbol{\phi}^\dagger_n$ is the solution of the adjoint problem $(ni\omega_c\mathcal{I}_1+\mathcal{L}^\dagger_n)\boldsymbol{\phi}^\dagger_n=0$ defined in Sec. IV. To obtain $\boldsymbol{\phi}^\dagger_0$, we eliminate $\pi^\dagger_0$ from the equation $\mathcal{L}^\dagger_0\boldsymbol{\phi}^\dagger_0=0$. To obtain $\boldsymbol{\phi}^\dagger_1$, we eliminate $u^\dagger_1$ and $\pi^\dagger_1$ from the equation $(i\omega_c\mathcal{I}_1+\mathcal{L}^\dagger_1)\boldsymbol{\phi}^\dagger_1=0$. We then numerically solve the resultant equations.

[1] H. Moffat and K. F. Jensen, J. Cryst. Growth **77**, 108 (1986).
[2] K. S. Gage and W. H. Reid, J. Fluid Mech. **33**, 21 (1968).
[3] R. E. Kelly, Adv. Appl. Mech. **31**, 35 (1994).
[4] K. Fujimura and R. E. Kelly, Phys. Fluids **7**, 68 (1995).
[5] S. H. Davis, J. Fluid Mech. **30**, 465 (1967).
[6] R. P. Davies-Jones, J. Fluid Mech. **44**, 695 (1970).
[7] J. K. Platten and J. C. Legros, *Convection in Liquids* (Springer-Verlag, Berlin, 1983), Chap. VIII, Sec. 4, pp. 556–564.
[8] J. Yamada, T. Miyazaki, and I. Hosokawa, J. Jpn. Soc. Fluid Mech. **15**, 417 (1996) (in Japanese).
[9] J. M. Luijkx and J. K. Platten, J. Non-Equilib. Thermodyn. **6**,

141 (1981).
[10] N. Y. Lee, W. W. Schultz, and J. P. Boyd, Int. J. Heat Mass Transf. **32**, 513 (1989).
[11] J. Mizushima, J. Phys. Soc. Jpn. **64**, 2420 (1995).
[12] T. Tatsumi and T. Yoshimura, J. Fluid Mech. **212**, 437 (1990).
[13] H. R. Brand, R. J. Deissler, and G. Ahlers, Phys. Rev. A **43**, 4262 (1991).
[14] H. W. Müller, M. Tveitereid, and S. Trainoff, Phys. Rev. E **48**, 263 (1993).
[15] M. T. Ouazzani, J. K. Platten, and A. Mojtabi, Int. J. Heat Mass Transf. **33**, 1417 (1990).
[16] M. T. Ouazzani, J. K. Platten, and A. Mojtabi, Appl. Sci. Res. **51**, 677 (1993).
[17] J. Guckenheimer and P. Holmes, *Nonlinear Oscillations, Dynamical Systems, and Bifurcations of Vector Fields* (Springer-Verlag, Berlin, 1983), The types 1–4 in Table V correspond to the cases Ib, II, V, and VIa in Table 7.5.2 of [17].